https://doi.org/10.5194/egusphere-2026-4721
Preprint. Discussion started: 22 September 2026

The Ross Ice Shelf airstream: How Ross Sea cyclone activity leads to winter-time sea ice breakout events in McMurdo Sound in the years 2013–2024

Mel Fülster[1,2], Ruzica Dadic[1], Iris Thurnherr[2], and Heini Wernli[2]

[1]WSL Swiss Federal Institute for Snow and Avalanche Research SLF
[2]Institute for Atmospheric and Climate Science, ETH Zürich

Correspondence: Mel Fülster (mfuelster@ethz.ch)

Abstract. Antarctic sea ice extent has shown increased variability since 2014. Although this variability has been attributed to a combination of oceanic and atmospheric forcings, considerable uncertainties remain. In coastal Antarctica, an important source of sea ice variability is the formation of polynyas and outbreaks of landfast sea ice, which are both influenced by complex atmospheric processes. While these processes can strongly impact regional sea ice variability, the links between large-scale atmospheric dynamics and regional sea ice extent remain incompletely understood. To address this gap, we investigate the sea ice extent in the McMurdo Sound during 2013–2024 using sea ice concentration data from the Japanese JAXA's GCOM-W1 satellite. More specifically, the study first introduces a pragmatic approach to identify polynya opening and fast ice breakout events from the satellite data (the sum of them referred to as "breakout events") and then investigates local atmospheric flow anomalies and large-scale dynamical processes that influenced the interannual variability of breakout events. The results show that (i) the total number of breakout events varies between 3 and 8 per winter period (April to August), with mainly polynya openings until 2018 and mainly fast ice breakout events in the later years; (ii) in agreement with previous studies, breakout events are associated with strong southerly winds (typically >10 m s^{-1}) (iii) breakout events are further associated with warm anomalies of about 8 K at Marble Point, a weather station close to the fast ice edge in McMurdo Sound; (iv) breakout events are related to the formation of the Ross Ice Shelf airstream, which is a barrier wind regime extending over more than 500 km along the Transantarctic Mountains; (v) breakout events (and the Ross Ice Shelf airstream) occur in response to enhanced large-scale sea level pressure gradients induced by (intense) cyclones in the Ross Sea; and (vi) the winter-mean frequency of Ross Sea cyclones correlates highly with the number of breakout events per winter. Together, our results reveal how large-scale atmospheric dynamics, particularly the frequency and intensity of Ross Sea cyclones, drive the formation and frequency of sea ice outbreak events and thus interannual sea ice variability in McMurdo Sound.

1 Introduction

The global climate is greatly affected by the spatial and temporal variability of sea ice. For example, declining sea ice cover increases absorbed solar energy at the ocean surface, with strong implications for Earth's radiative energy budget (Pistone et al., 2014). Furthermore, sea ice formation is a significant driver of the global ocean circulation (Stössel et al., 2002; Jacobs,

https://doi.org/10.5194/egusphere-2026-4721
Preprint. Discussion started: 22 September 2026

2004; Tamura et al., 2008, 2016). Antarctic sea ice extent varies seasonally, expanding during the Southern Hemisphere winter and retreating in summer. Antarctic sea ice covers on average ~ 18.5 million km^2 in late winter. This area is reduced to approximately 2.5 million km^2 in the summer seasons (National Snow and Ice Data Center, 2024). Satellite records reveal that the yearly average sea ice extent in Antarctica gradually increased from the 1970s to 2014, unlike the Arctic sea ice, which has been experiencing a continuous reduction of sea ice area for more than three decades (Parkinson, 2019). However, within only three years (2014–2017) the Antarctic sea ice extent declined drastically, comparable to 30 years of sea ice loss in the Arctic (Parkinson, 2019; Eayrs et al., 2021). The sea ice extent at both Poles continues declining, with new record low Antarctic sea ice extents in both summer and winter recorded in 2023 (Roach and Meier, 2024). The drastic variability in sea ice extent after 2014 can partly be explained by a combination of atmospheric and oceanic forcings (Turner et al., 2017; Stuecker et al., 2017; Schlosser et al., 2018; Wang et al., 2019; Meehl et al., 2019) but our understanding of the main factors influencing sea ice variability remains incomplete.

About 10% of total Antarctic sea ice is produced in polynyas, areas of open water surrounded by sea ice often called sea ice factories (Tamura et al., 2008, 2016; Fraser et al., 2019; Wei et al., 2021; Golledge et al., 2025). In Antarctica, the highest ice production occurs in the Ross Ice Shelf Polynya region, which includes the Ross Sea Polynya, the Terra Nova Polynya, and the McMurdo Sound polynya (Tamura et al., 2008; Burada et al., 2023). Not only are polynyas essential in sea ice production, but they also play an important role in ocean dynamics, biological and biogeochemical processes (Fraser et al., 2019; Wei et al., 2021; Fraser et al., 2023; Golledge et al., 2025). For example, brine rejection during ice formation in polynyas leads to saltier and colder water, which drives deep-water formation, contributing to the production of Antarctic Bottom Water and thus the Global Meridional Overturning Circulation and ocean dynamics (Stössel et al., 2002; Jacobs, 2004; Tamura et al., 2008). The lack of a thick ice or snow cover in a polynya allows light to penetrate further into the water, increasing primary productivity, which in turn provides the nutrition many animals need (Arrigo and Van Dijken, 2003; Wei et al., 2021; Golledge et al., 2025). To understand the interannual variability in deep-water formation and ecological processes, it is therefore crucial to understand the causes of interannual variability of polynyas.

Many coastal polynyas, such as the McMurdo Sound polynya, are found between pack and landfast sea ice (for example, Fig. 1b). Landfast sea ice, often just called fast ice, is sea ice that is attached to or fastened to grounded icebergs, continents, or ice shelves. Because the polynyas often share a boundary with fast ice, they should be considered an inherently coupled system: variability in the fast ice edge impacts the size and location of coastal polynyas (Wei et al., 2021), and, in turn, coastal polynyas influence the fast ice edge (Nihashi and Ohshima, 2015) as well as fast ice thickness (Langhorne et al., 2023). The interaction between fast ice and polynyas is discussed in Fraser et al. (2019) for the Cape Darnley polynya and Massom et al. (2001) for the Mertz Glacier polynya. Tamura et al. (2016) showed that changes in the location of fast ice impacted the sea ice production in the Ross Sea and Mertz Glacier polynyas. In other words, to identify the drivers of variability of polynyas and sea ice production in Antarctica, it is essential to understand the variability and anomalies of the fast ice extent.

Here, we focus on sea ice in the McMurdo Sound, a small bay in the western part of the Ross Sea, Antarctica, characterised by a combination of pack ice of free floating ice floes, and fast ice (Fig. 1b). The majority of the sea ice in McMurdo Sound is seasonal fast ice (Kim et al., 2018), which is important for station operations at McMurdo Station and Scott Base. Fast ice

https://doi.org/10.5194/egusphere-2026-4721
Preprint. Discussion started: 22 September 2026

in McMurdo Sound mainly forms through thermodynamic processes. The presence of supercooled water allows the fast ice to grow not only due to heat loss to the atmosphere, but also through heat loss to the ocean (Richter et al., 2024).

In a normal year, the sea ice in McMurdo Sound reaches its minimum in February/March and increases during winter before it breaks up the following January. Around February, at the end of the Southern Hemisphere summer, McMurdo Sound is almost completely ice-free. The fast ice forms in March–April with its edge extending to $\sim 77.6°$S (Kim et al., 2018; Fraser et al., 2023). At its maximum extent, the fast ice spans the entire Sound. Usually, the fast ice starts an initial retreat between September and November. At this time, the polynya in McMurdo Sound becomes very active, meaning it opens and freezes often (Price, 2014). In January, the fast ice starts its final retreat until it once again reaches its minimum extent in February. In some years, however, repeated sea ice breakouts prevent the formation of a stable ice cover until later into the winter season, which can affect the local polynya as well as field work on the sea ice (Leonard et al., 2021). In 2022 and 2024, repeated sea ice breakouts in winter also impacted station operations. Leonard et al. (2021) established a connection between these sea ice breakout events and strong southerly wind events in McMurdo Sound during winter 2019. More recently, Radlwimmer et al. (2026) discussed the increased winter storminess in McMurdo Sound between 1964 and 2024, but they emphasized the need for a direct link between temperature anomalies and low-pressure systems in the Ross Sea.

The local atmospheric flow system on the Ross Ice Shelf has been studied in great detail. Radiative cooling during the austral winter leads to extremely stable stratification in the lower levels of the atmosphere above the Ross Ice Shelf. There are two main mechanisms that can move this stably stratified air across the ice shelf: (i) katabatic drainage flows, which occur when air from the Antarctic Ice Sheets flows downslope onto ice shelves or towards the Antarctic coast, and (ii) cyclonic advection by extratropical cyclones in the Ross Sea (Parish et al., 2006). The large-scale pressure field associated with the presence of a cyclone north of the Ross Ice Shelf reinforces continental drainage flows (Fig. 1a, small red arrows). Furthermore, the cyclonic circulation forces the cold and stably stratified air on the Ross ice shelf against the Transantarctic Mountains, leading to cold air damming or blocking. Associated with this blocking is a horizontal pressure gradient oriented away from the mountain range, which, if it persists long enough, will cause a barrier wind along the Transantarctic Mountains (O'Connor et al., 1994; Parish et al., 2006; Seefeldt and Cassano, 2012). In this case, the barrier wind is a low-level, northward-directed airstream on the Ross Ice Shelf, known as the Ross Ice Shelf airstream (Parish et al., 2006; Seefeldt and Cassano, 2012).

While a component of the Ross Ice Shelf airstream is made up of katabatically forced continental drainage flows, the air stream is primarily associated with a cyclone in the Ross Sea whose intensity and position determine the spatial extent and intensity of the airstream (Parish et al., 2006; Seefeldt and Cassano, 2012). Several studies discussed the relationship between Antarctic sea ice variability and extratropical cyclones, noting that the 10 m wind associated with these weather systems is the primary atmospheric dynamic driver of sea ice variability (e.g., Holland et al., 2017; Schemm, 2018; Zhong et al., 2025). The Southern Ocean storm track around Antarctica, defined as the region of relatively high cyclone frequency, has three local maxima. In winter (June–August) these are in the high-latitude south Indian Ocean and in the Amundsen and Ross Seas (Papritz et al., 2014). Even though it has been noted that cyclone passages through the Ross Sea region in June, July, and August contribute greatly to the large-scale flow dynamics on the Ross Ice Shelf (O'Connor and Bromwich, 1988; O'Connor

https://doi.org/10.5194/egusphere-2026-4721
Preprint. Discussion started: 22 September 2026

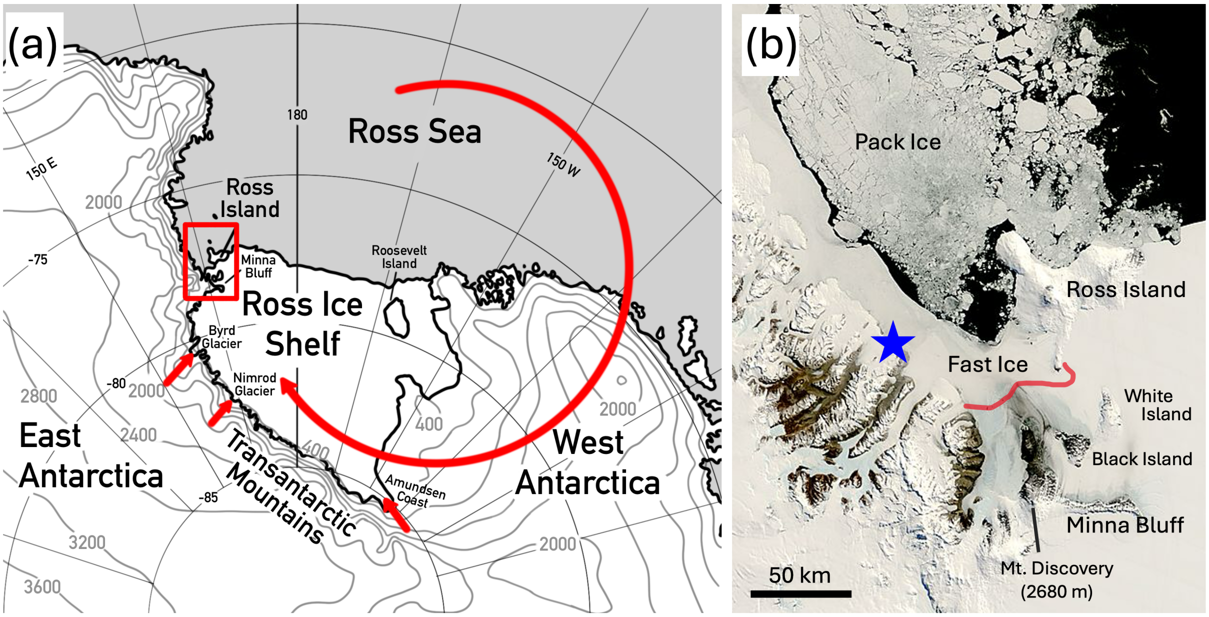

Figure 1. **a** The Ross Ice Shelf region. Shaded in grey are the Ross Sea and the Southern Ocean. Thick grey lines show terrain height (in m). The short red arrows indicate the location of glacial valleys through which cold air can drain from the Antarctic Ice Sheets onto the Ross Ice Shelf. The large curved arrow illustrates how a cyclone in the Ross Sea can advect air towards the Transantarctic Mountains. **b** Representative MODIS image of the McMurdo Sound region indicated by the red box in **a** on 12 December 2007 (NASA Worldview Snapshots, 2007). The blue star shows the location of the Marble Point automatic weather station. The red line approximately indicates the southern border of McMurdo Sound with the Antarctic Continent and the Ross Ice Shelf. The ice north of the red line is landfast sea ice (fast ice). Between the fast and pack ice is a small polynya. South of McMurdo Sound is Minna Bluff, a peninsula attached to the Transantarctic Mountains. Its highest peak is Mount Discovery at 2 680 m a.s.l.

et al., 1994; Parish et al., 2006; Seefeldt and Cassano, 2012), the impact of such weather systems on the local wind system in McMurdo Sound and its implication for sea ice variability have not been studied in detail.

Southerly flow from the Ross Ice Shelf is often blocked at the southern entrance of McMurdo Sound by Minna Bluff (Fig. 1b). Due to this orographic flow blocking, southerly winds from the Ross Ice Shelf are usually directed around Minna Bluff (O'Connor and Bromwich, 1988; Seefeldt et al., 2003). However, at high enough wind speeds, they can also flow over Minna Bluff into McMurdo Sound, causing strong wind events that are responsible for ice breakout and polynya openings (O'Connor and Bromwich, 1988). While a link between the local wind system and breakout events has been established for 2019 (Leonard et al., 2021), the direct connection between large-scale atmospheric processes and the daily and interannual variability of fast ice in McMurdo Sound has yet to be established.

This study aims to improve understanding of the atmospheric processes that govern coastal sea ice variability in McMurdo Sound by investigating the link between sea ice breakout events and large-scale atmosphere dynamics over the Ross Ice Shelf and in the Ross Sea. We do this by identifying and classifying changes in fast ice extent and the McMurdo Sound polynya,

https://doi.org/10.5194/egusphere-2026-4721
Preprint. Discussion started: 22 September 2026

and comparing this variability with local temperature and wind measurements. To determine what role large-scale atmospheric dynamics play in the formation of breakout events and in interannual variability of fast ice, we analyse pressure, temperature, and wind fields from local weather stations and discuss cyclone activity (identified from reanalysis data) in the Ross Sea. Finally, we comment on the delayed formation of a stable fast ice cover in the years 2019, 2022, and 2024.

2 Data and methods

2.1 Identification of breakout events based on sea ice fraction

To quantify changes in winter (April–August) fast ice cover in McMurdo Sound, a regional sea ice fraction (SIF) is calculated. This SIF is based on sea ice concentration from the satellite-derived AMSR2/ARTIST sea ice data set (Spreen et al., 2008). The AMSR2 Sensor was launched to space by the Japanese space agency JAXA in May 2012. The first full year of observations was 2013 and the measurements are ongoing. The relatively high spatial resolution of the AMSR2/ARTIST product is particularly suitable for capturing changes in the sea ice concentration on the small spatial scale of McMurdo Sound, which sets it apart from other similar satellite products, but limits our analysis to the years 2013–2024.

Within the perimeters of the box shown in Fig. 2, each pixel has a size of $3.125\,\mathrm{km} \times 3.125\,\mathrm{km}$. The total number of pixels within the box varies from day to day, due to small changes in the land mask[1]. The daily SIF in McMurdo Sound, SIF_{all}, is the fraction of pixels within the box with a sea ice concentration $\geq 15\,\%$ (following the method described by Leonard et al., 2021). Additionally, SIF_{coast} has been defined, calculated using only pixels south of 77.6°S. SIF_{coast} is used to identify changes in the fast ice extent, while SIF_{all} includes polynya openings *and* changes in the fast ice extent. We restrict our analysis to the period from 1 April to 31 August of each year. Since fast ice is frequently still developing in early April the effective start date of the data analysed is delayed in 2014, 2016, 2017, 2018, 2020, 2021, and 2024 until the fast ice has fully formed. For the effective start dates in those years refer to Table A1 in the Appendix.

For this study we introduce a distinction between two types of breakout events: polynya openings (POs) and fast ice breakout events (FIBEs). A PO does not affect the extent and stability of the fast ice cover in McMurdo Sound, whereas during a FIBE, as the name implies, the fast ice breaks out, and the fast ice edge shifts south of 77.6°S. Quantitatively, this is captured by differences in the SIFs: during FIBEs both SIFs (SIF_{all} and SIF_{coast}) are low (see example in Fig. 2a), whereas during POs SIF_{all} is low while SIF_{coast} remains high (Fig. 2b). According to our definition, a breakout event can only either be a FIBE or a PO, and so the total number of breakout events is equal to the sum of all FIBEs and POs.

We define that a breakout event starts at the last time step when both SIFs are still > 0.95. The end of a breakout event is when both SIFs are again > 0.95 for more than one time step (one day). During a breakout event, at least one SIF must drop below 0.9 at least once. This threshold is applied to filter changes in sea ice cover that do not significantly impact the overall stability of the fast ice cover in McMurdo Sound. With this definition any time series can be split into “event” and “non-event” periods, referring to time periods that coincide with breakout events in McMurdo Sound and those that do not. A non-event

[1] Since this variability is constrained to a small number of pixels it does not affect the results of the SIF analysis.

https://doi.org/10.5194/egusphere-2026-4721
Preprint. Discussion started: 22 September 2026

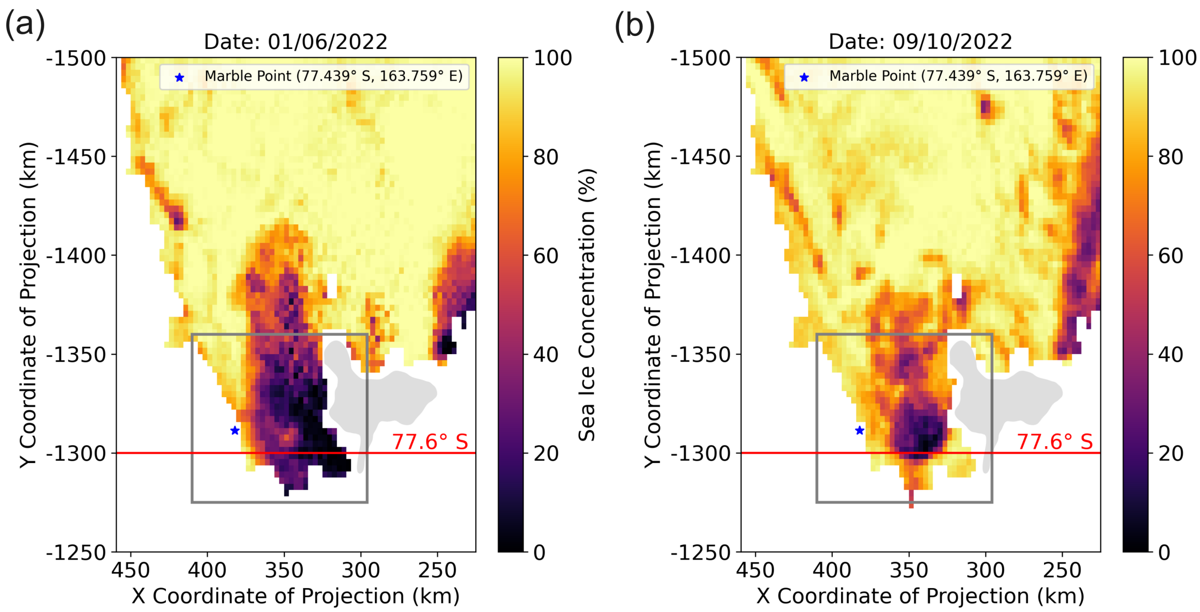

Figure 2. ASI sea ice concentration in polar stereographic projection in McMurdo Sound for (**a**) a fast ice breakout event with SIF_{coast}=0.585 on 1 June 2022 and (**b**) a polynya opening with SIF_{coast}=0.976 on 9 October 2022. The Antarctic land mask is shown in white with a rough outline of Ross Island superposed in grey shading. The grey box marks the area used to calculate SIF_{all}, while the red line at 77.6°S represents the approximate fast ice edge in McMurdo Sound used for the calculation of SIF_{coast}. The blue star indicates the location of the Marble Point automatic weather station.

starts on the day the preceding breakout event ended and ends when the next breakout event starts. Table A1 in the Appendix lists the identified breakout event days and non-event days for April–August in the years 2013-2024.

Leonard et al. (2021) compared the changes in the daily SIF to two other methods for determining the sea ice cover in McMurdo Sound. They verified that changes in SIF coincide with breakout events as identified by SAR and MODIS. Therefore, despite its simplicity, this method based on SIF is suitable for the analyses discussed in this paper.

2.2 In situ meteorological measurements in McMurdo Sound

We use data from Marble Point (blue star in Fig. 2) due to its public availability (Antarctic Meteorological Research and Data Center, 2024), high quality, and the station's proximity to the fast ice edge. The Marble Point weather station is located at 77.439°S, 163.754°E, only ∼20 km away from the fast ice edge in McMurdo Sound at 77.6°S (Leonard et al., 2021), and 108 m above mean sea level. The daily observations include measurements of temperature, pressure, wind speed and direction at 10-minute intervals. Our analysis is limited to the years 2013–2024 due to the availability of the sea ice concentration data, however a climatology of temperature at Marble Point was calculated with data from 1991–2024.

https://doi.org/10.5194/egusphere-2026-4721
Preprint. Discussion started: 22 September 2026

2.3 ERA5

ERA5 is the latest release of the reanalysis dataset of the European Centre for Medium-Range Weather Forecasts (ECMWF) (Hersbach et al., 2020). The temporally homogenous dataset is derived from a combination of model data and observations. ERA5 provides hourly data of a vast number of atmospheric, land, and oceanic variables from 1940 to present but due to a lack of observations, ERA5 is unreliable at high southern latitudes before 1979. We use the variables at a horizontal resolution of $0.5° \times 0.5°$, and a vertical extent from the surface up to a height of 30 km, with data on 98 vertical levels.

2.3.1 Trajectory analysis

The three-dimensional wind fields from ERA5 were used with the Lagrangian analysis tool LAGRANTO (Wernli and Davies, 1997; Sprenger and Wernli, 2015) to calculate 4-day backward trajectories from McMurdo Sound during breakout events. For each breakout event, five sets of 20 trajectories were started, each separated by an hour, with the third set of trajectories coinciding with peak winds observed at Marble Point during the start of a breakout event. For example, for a breakout event on 30 March 2022, the peak winds were observed at 15:00 UTC. Five sets of trajectories were then started at 13:00 UTC, 14:00 UTC, 15:00 UTC, 16:00 UTC, and 17:00 UTC. The starting points of the trajectories were spaced 15 km apart, in a box ranging from 164°E to 167°E, and 77.25°S to 77.75°S. The trajectories were started at 25 hPa above ground level. The coordinates of the trajectories (longitude, latitude, and pressure) were output every hour.

2.3.2 Weather maps and cyclone identification

Composites, i.e., averages of selected ERA5 fields are calculated for event and non-event days determined by the McMurdo Sound sea ice fractions.

Cyclone frequencies were calculated in ERA5 with a refined version of the algorithm developed by Wernli and Schwierz (2006), as described in Sprenger et al. (2017). Here, cyclones are defined as the finite area that surrounds a local sea-level pressure (SLP) minimum and is enclosed by the outermost closed SLP contour. For each identified cyclone, hourly cyclone masks were determined covering these cyclone areas. The time average of the cyclone mask provides a cyclone frequency for that time period at each grid point (Fig. 3a), indicating how often there was a cyclone over a given grid point in a given period. The cyclone mask is also used to determine the minimum SLP associated with a cyclone passing through the Ross Sea sector, which is defined as the region of highest cyclone frequency in the Ross Sea (black dashed line in Fig. 3). At one-hourly intervals, if there is a cyclone within the sector, the minimum SLP of that cyclone within the sector is extracted (yellow star in Fig. 3b,c). Note that at times the minimum SLP extracted will not be the true minimum SLP of the cyclone, but rather the lowest SLP within the sector (compare to Fig. 3c). Limiting the minimum SLP to the area within the sector ensures that the minimum SLP is an indicator of whether it can have a strong impact on the air flow on the Ross Ice Shelf. If only a small part of the cyclone mask is within the sector, the minimum SLP extracted for this cyclone will only differ slightly from the background SLP.

https://doi.org/10.5194/egusphere-2026-4721
Preprint. Discussion started: 22 September 2026

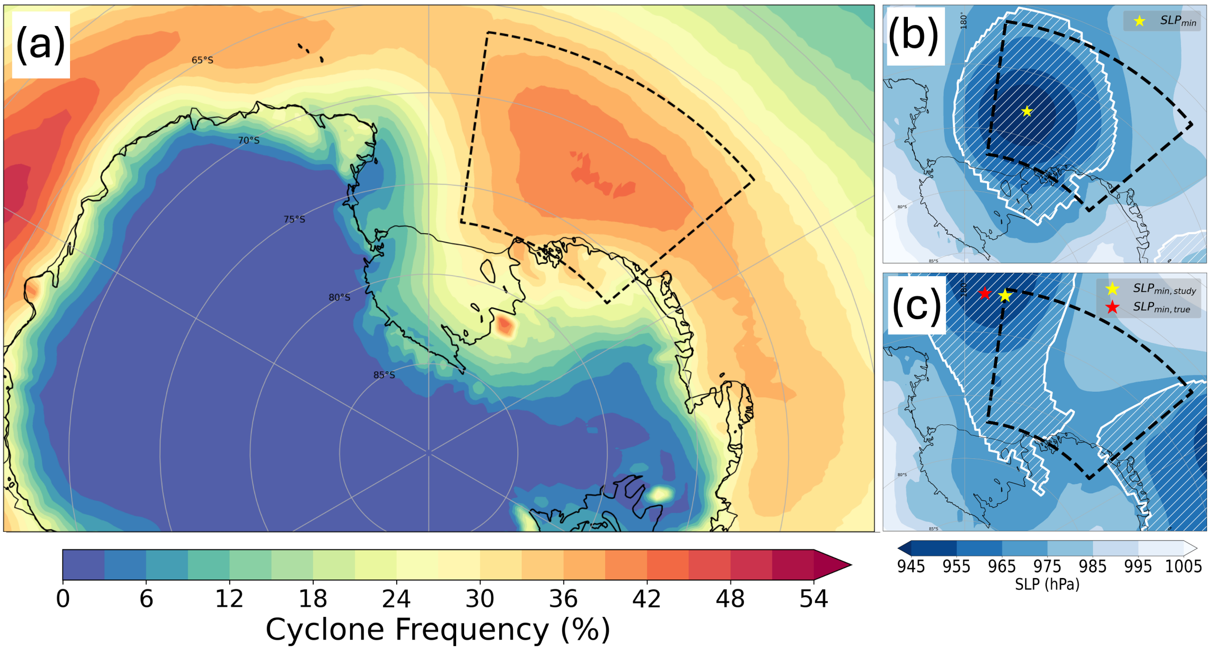

Figure 3. (a) Climatological cyclone frequency distribution (in %) surrounding the Ross Sea for the months April to August during 2013–2024. The Antarctic continent is outlined in black. The dashed black box denotes a Ross Sea sector that includes the climatological cyclone frequency maximum in the Ross Sea; it is used to calculate time series of cyclone frequency and SLP minima. **(b), (c)** examples illustrating how SLP minima in the outlined sector are identified. Colours show SLP (in hPa), the white hashing indicates the location of the cyclone mask, and the yellow star indicates the SLP minimum used in our study. The red star in **(c)** indicates the cyclones true SLP minimum, which is located outside of the sector.

3 Results and discussion

3.1 Sea ice variability

In this section we first provide a general overview of the sea ice variability in McMurdo Sound from 2013–2024, including seasonal patterns. SIF_{all} and SIF_{coast} show an overall similar seasonal cycle (Fig. 4). Every year, there is a minimum in sea ice coverage in Southern Hemisphere summer around February to March, with SIF_{all} declining in January to February, while SIF_{coast} follows with a delay of 1-2 months. In March, SIF_{all} increases simultaneously to SIF_{coast} until it reaches a value of 1 (full coverage) in April to May. In the winter period from June to August there may be some breakout events, but in all years (2013–2024) SIF_{all} and SIF_{coast} return to a value of 1 between April and August, i.e., McMurdo Sound always freezes over again. In September to October the polynya becomes very active (e.g., variability of SIF_{all} (grey) in 2015, Fig. 4); it opens often and does not always completely freeze over before the sea ice starts its final retreat in January again. This overall behaviour of SIF_{all} and SIF_{coast} is in agreement with the climatological behaviour of fast ice in McMurdo Sound described by Kim et al. (2018).

https://doi.org/10.5194/egusphere-2026-4721
Preprint. Discussion started: 22 September 2026

Several years show contrasting behaviour in their polynya activity during winter. In the years 2013-2018, 2021, and 2023 SIF_{coast} is mostly constant and equal to 1 from April to August (Fig. 4, black lines). However, there is some variability in SIF_{all} during these months (Fig. 4, grey lines). This indicates that the McMurdo Sound polynya opens regularly, while the fast ice generally stays intact, i.e., there are POs but no FIBEs. In contrast, in 2019, 2022, and 2024 there is variability in both SIF_{all} *and* SIF_{coast} (Fig. 4, purple highlights) with SIF_{coast} decreasing below 60% more than once during winter. This means that the fast ice cover, which is usually stable from April to August, is impacted by FIBEs in McMurdo Sound in these years. SIF_{coast} in 2020 indicates that the fast ice was also unstable in this winter, however, this variation is more continuous and has a smaller magnitude than in 2019, 2022 and 2024. Since there were no station accounts of unstable fast ice in 2020 this could indicate that the 2020 McMurdo Sound polynya was larger and more active, without impacting the stability of the fast ice closer to the Ross Ice Shelf and the research stations on Ross Island. Some FIBEs are observed in 2013-2018, 2021, and 2023, but they tend to occur earlier in the winter season, are smaller, less frequent, and did not have an impact on the overall stability of the fast ice cover.

Over the 12 year record from 2013-2024, there is no statistically significant trend in the overall number of breakout events (black squares in Fig. 5a). However, from 2013-2018 (the first 6 years of the record) most breakout events are POs, whereas from 2019-2024 (the second 6 years of the record) the breakout events are mostly FIBEs. Assuming that FIBEs always result in a larger polynya area than POs (see Fig. 2), this regime shift implies that the McMurdo Sound polynya area was increasing from 2013 to 2024. In general, the area of coastal polynyas in the Ross Sea has been increasing over the past 44 years (Duffy et al., 2024), and Yang et al. (2025) showed that winter polynya area was increasing in Antarctica from 2013 to 2022. Burada et al. (2023) observed high polynya areas in McMurdo Sound for the year 2019, a year in which there were many wintertime FIBEs as shown in Fig. 5a and as discussed in Leonard et al. (2021). Our results confirm these observations, and thus demonstrate that the definition of POs and FIBEs, as used in this study, represents the sea ice variability in the McMurdo Sound well.

3.2 Local weather at Marble Point, McMurdo Sound

To connect the sea ice variability in McMurdo Sound to the large-scale atmospheric dynamics, it is important to understand how the local weather in McMurdo Sound is related to the winter-time breakout events (POs and FIBEs in April to August) discussed in the previous section. Figure 6 compares the SIF time series (SIF_{all} and SIF_{coast}) with wind and temperature measurements from Marble Point for one specific winter (April–August 2021). Both FIBEs and POs coincide with strong winds ($> 10\,\mathrm{m\,s^{-1}}$, highlighted in red in Fig. 6) from a south, south–easterly direction. Leonard et al. (2021) also identified that southerly strong wind events led to fast ice breakout events in 2019. From a local perspective, southerly winds are expected to advect cold air from the Antarctic continent. However, Fig. 6d indicates that leading up to the southerly strong wind events air temperatures are increasing, often leading to positive temperature anomalies above the climatological 90th percentile.While the positive temperature anomalies are up to $+15°\mathrm{C}$, the absolute temperatures stay consistently below $0°\mathrm{C}$ (Fig. 6d). The duration of the events is too short to significantly warm and weaken the sea ice, even if the air temperatures were above $0°\mathrm{C}$, indicating that the winds are not melting the fast ice, but must be breaking it up mechanically.

https://doi.org/10.5194/egusphere-2026-4721
Preprint. Discussion started: 22 September 2026

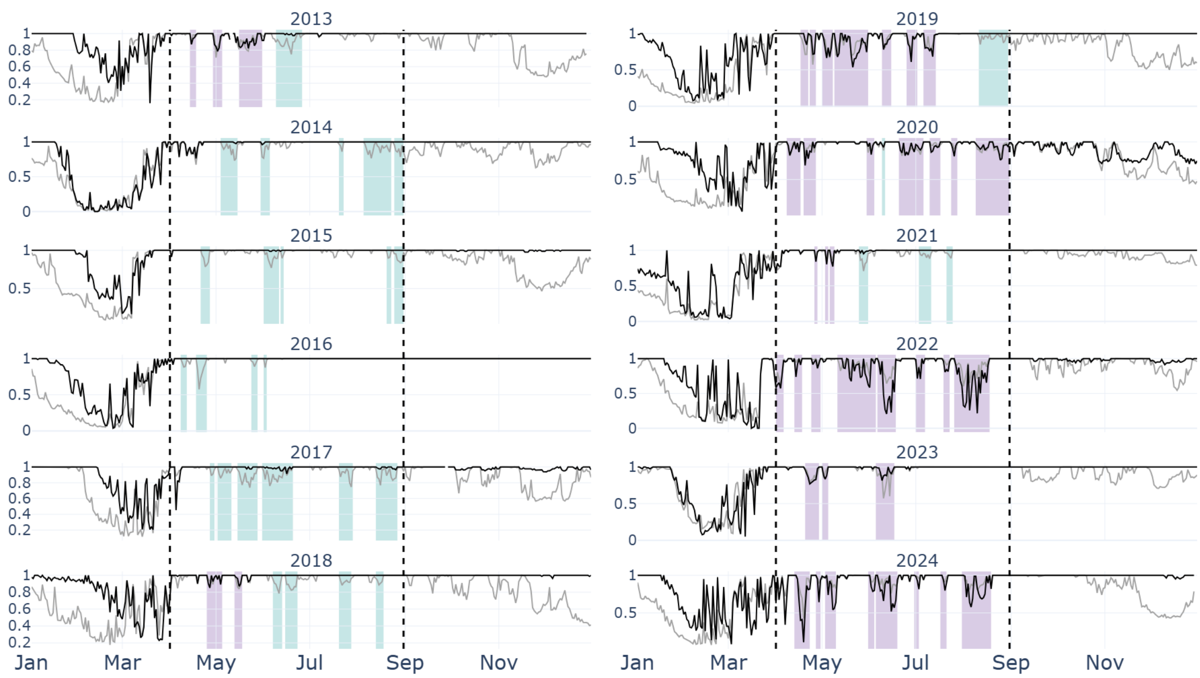

Figure 4. Time series of daily SIF for the years 2013–2024 averaged in the entire McMurdo Sound (SIF$_{all}$, grey), and the smaller region south of 77.6°S (SIF$_{coast}$, black) as indicated in Fig. 2. Vertical dashed black lines indicate the time frame of interest (1 April–31 August). Within this time frame purple shading highlights FIBEs and turquoise shading indicates POs. See text for details.

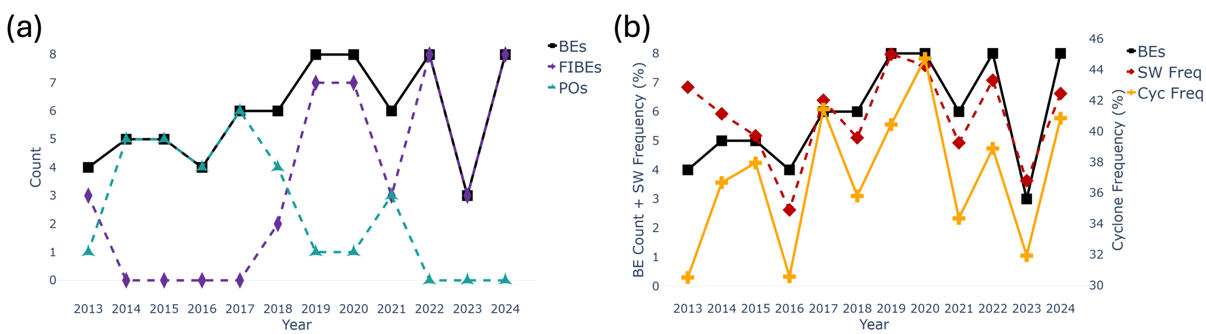

Figure 5. (a) Time series of the number of breakout events (black squares), FIBEs (purple diamonds), and POs (turquoise triangles) that occurred per year in 2013–2024. **(b)** A comparison of the annual number of breakout events (black squares), the strong wind (SW) frequency (red diamonds), and the winter-mean cyclone frequency in the sector defined in Fig. 3a (yellow crosses) from April to August, 2013–2024.

https://doi.org/10.5194/egusphere-2026-4721
Preprint. Discussion started: 22 September 2026

Similar results are seen for breakout events in all years 2013–2024 (e.g. Fig. 7 for the year 2022): breakout events, whether FIBEs or POs, coincide with strong southerly winds and are often accompanied by positive temperature anomalies. A comparison of the temperature distribution at Marble Point during breakout events and at times when the fast ice stays intact confirms the warm anomaly during breakout events with a $8.1°C$ mean difference, which is larger than the 1σ-range, between breakout and non-breakout events (Fig. 8). According to Stefan's law (Stefan, 1891), the thermodynamic growth rate of sea ice is proportional to the temperature difference between the ocean and sea ice surface. Assuming that the sea ice surface temperature is proportional to the 2-m temperature this means, while the absolute temperatures during a breakout event in McMurdo Sound are not high enough to melt the ice, they would have thermodynamic implications for the sea ice production after the McMurdo Sound polynya opens, i.e., how fast it freezes again.

Figure 9 shows the distributions of wind measurements at Marble Point during events and non-events. Considering all measurements, wind vectors have a small northerly component when the fast ice stays intact (non-events, Fig. 9b), but during breakout events the winds always blow from a southerly direction (Fig. 9a). On average, the wind speeds are lower during non-events (average wind speed $3.5\,\mathrm{m\,s^{-1}}$) than during breakout events (average wind speed $5.3\,\mathrm{m\,s^{-1}}$), which is also seen by the smaller frequency of winds greater than $10\,\mathrm{m\,s^{-1}}$ in Fig. 9e and f.

The overall higher wind speed during events is also reflected in the 90th percentile, which is $10.8\,\mathrm{m\,s^{-1}}$ for events and $7.4\,\mathrm{m\,s^{-1}}$ for non-events. Winds during non-events above the 90th percentile mostly originate from a south-easterly direction (Fig. 9d). In comparison, the wind directions during events spread from southerly to south-easterly, with the highest frequency seen for southerly winds (Fig. 9c). The effect of low and high wind speed events on the wind flow around Ross Island was also investigated by Seefeldt et al. (2003). They found that at times when the lower atmosphere was very stable and the wind speed low, the dominant wind direction at Marble Point was from south to south-easterly directions, with wind speeds consistently below $12.5\,\mathrm{m\,s^{-1}}$. During a typical high wind speed event on the other hand, the wind speeds were $> 10\,\mathrm{m\,s^{-1}}$ and blowing from the south in all parts of McMurdo Sound. In contrast to Seefeldt et al. (2003), in our 12-year dataset, high wind speed events, even though dominated by southerly wind direction, show also south-easterly flow (Fig. 9e,f). Note that there are only a few occasions with wind speed larger than $10\,\mathrm{m\,s^{-1}}$ for non-events (Fig. 9f) whereof all have a south-easterly direction.

A strong relationship between wind speed and sea ice breakout events can also been seen on an interannual time scale. There is a high correlation between the annual strong wind frequency, i.e., the fraction of wind measurements at Marble Point that are $> 10\,\mathrm{m\,s^{-1}}$ between April and August each year, and McMurdo breakout events (Fig. 5b) with a Pearson correlation coefficient of 0.75, and a Spearman correlation coefficient of 0.71. This result is in agreement with a multitude of studies that have shown that wind is one of the main forcing mechanisms of coastal polynya variability (Stössel et al., 2002; Dale et al., 2017; Huot et al., 2021; Wei et al., 2021; Fonseca et al., 2023). Having established a connection between local weather events and sea ice breakout events in McMurdo Sound, the following sections aim to connect these local weather events to large-scale atmospheric dynamics.

https://doi.org/10.5194/egusphere-2026-4721
Preprint. Discussion started: 22 September 2026

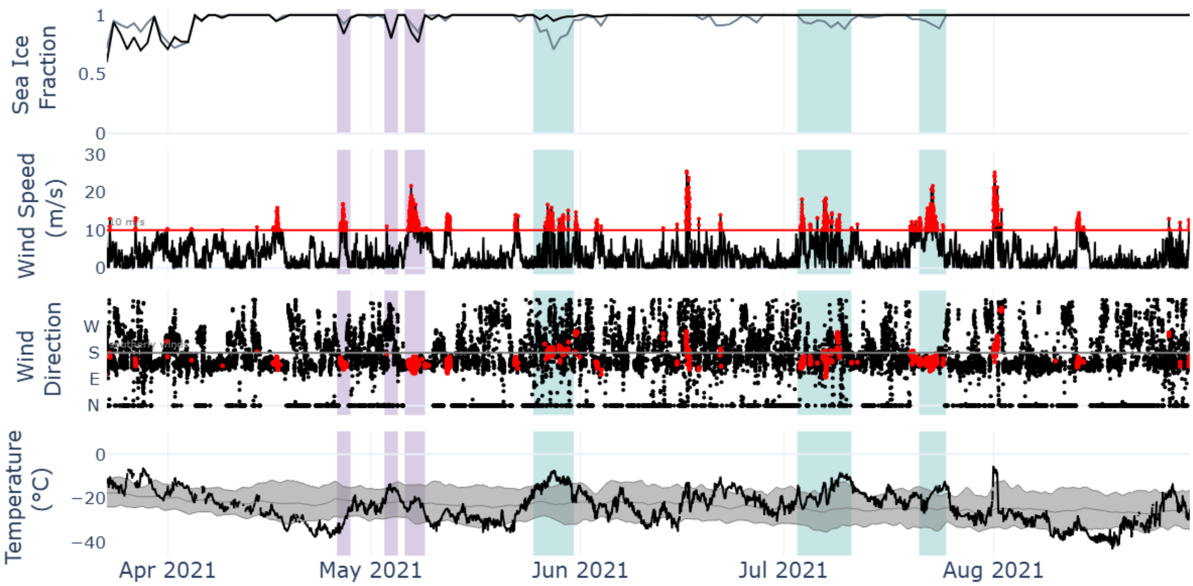

Figure 6. Time series of both SIFs and hourly measurements of wind and temperature at Marble Point from 23 March 2021 to 31 August 2021. The graph is in keeping with Figure 3 of the previous study of sea ice breakouts by Leonard et al. (2021) for a better comparison. FIBEs are highlighted in purple, POs in cyan. **(a)** SIF in McMurdo Sound in the larger region shown in Fig. 2 (SIF_{all}, grey) and in the smaller region south of 77.6°S (SIF_{coast}, black). **(b)** Wind speed in $m\,s^{-1}$; the red line indicates the threshold for strong winds at $10\,m\,s^{-1}$, and red markers highlight wind speeds exceeding the threshold; **(c)** Wind direction, red markers show again times with wind speeds exceeding the threshold and the grey horizontal line indicates southerly winds. **(d)** Surface air temperature (in °C, black) compared to the climatological mean (grey line) and the climatological 10th to 90th percentiles (grey shading). Climatological data (1991–2024) was smoothed using a 3-day window.

3.3 Lagrangian analysis of origin of event air parcels

To connect the local weather events responsible for breakout events in McMurdo Sound to large-scale atmospheric dynamics, the origin of air parcels contributing to strong wind events is investigated. For this purpose, backward trajectories were calculated between April and August each year from 2013–2024, as explained in Sect. 2.3.1. To evenly cover the identified outbreak event among the years, the same number of events per year were used for this analysis. We calculated trajectories for three breakout events each year, which was limited by the small number of breakout events in 2016. The three breakout events were chosen to be, as much as possible, equally spaced out in the winter season. For example, in a year with breakout events from April to June, one event was selected for April, May and June respectively. Additionally, trajectories for five "non-events" were calculated in each year. The times of the non-events were selected based on the following criteria:

- SIF_{all}=1 and SIF_{coast}=1,
- wind speed measurements at Marble Point $<10\,m\,s^{-1}$.

https://doi.org/10.5194/egusphere-2026-4721
Preprint. Discussion started: 22 September 2026

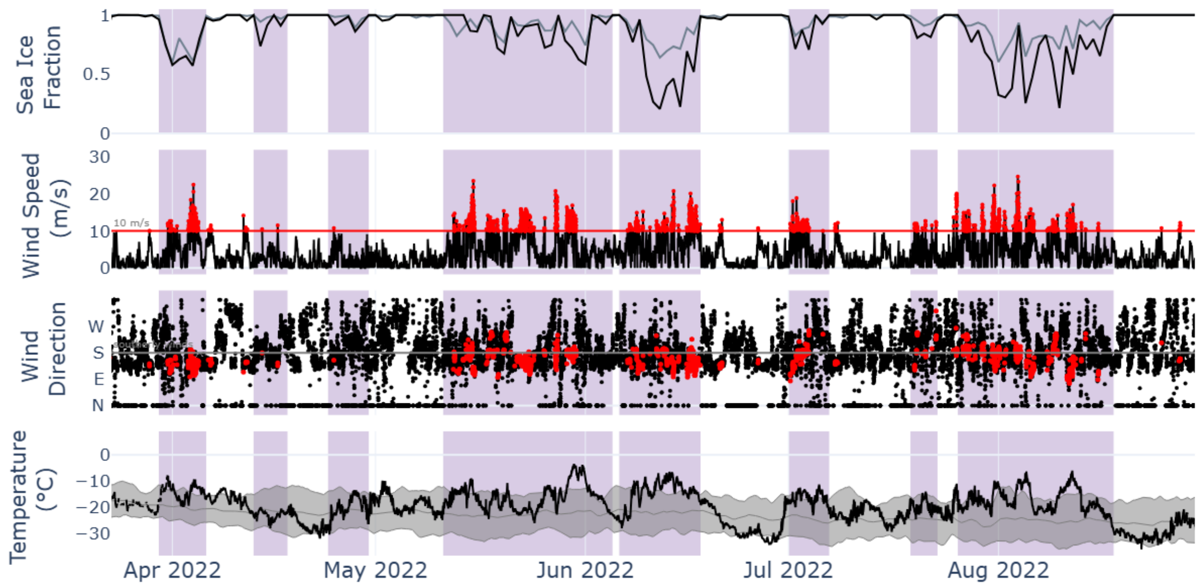

Figure 7. Same as Fig. 6 but for the year 2022.

The air parcel origin for events and non-events shows distinct differences. For the non-events (Fig. 10b), the air parcels approach McMurdo Sound relatively isotropically. While some trajectories extend a little further on the East and West Antarctic Ice Sheets, the majority stay close to McMurdo Sound, indicating that these air parcels moved slowly. This agrees with the local wind distribution discussed in Seefeldt et al. (2003) and the wind roses in Fig. 9 where the dominant wind direction during non-events is south-easterly, and wind speed rarely exceed $10\,\mathrm{m\,s^{-1}}$. As discussed in the introduction, at insufficient wind speeds, the air is not able to flow over the orography south of McMurdo Sound and are deflected around Minna Bluff and Ross Island (O'Connor and Bromwich, 1988; Chenoli et al., 2013).

The radial extent of trajectories connected to breakout events is much greater than for non-events (Fig. 10a). While some trajectories cross the entire West Antarctic Ice Shelf before a breakout event, most originate from lower latitudes in the Ross Sea. Since all trajectories for events and non-events are 4 days long, this indicates that air parcels travel much faster leading up to a breakout event. This is also supported by the wind distribution (Fig. 9), which shows a higher frequency of strong winds for breakout events than non-events. Furthermore, the air parcels during outbreak events (Fig. 10a) consistently approach McMurdo Sound from the south. The bright red-yellow band shows that up to 90% of all trajectories move along the Transantarctic Mountains. The air parcels approach the Transantarctic Mountains either from the eastern part of the Ross Sea or from the other side of the West Antarctic Ice Sheet. They are then directed northwards, and their high speed allows them to overcome the orographic blocking south of McMurdo Sound.

During sea ice breakout events, there is a pronounced area of high cyclone frequency in the Ross Sea (Fig. 10a, grey contours), which corresponds to a low SLP area with values below 980 hPa (not shown). During breakout events there also is

https://doi.org/10.5194/egusphere-2026-4721
Preprint. Discussion started: 22 September 2026

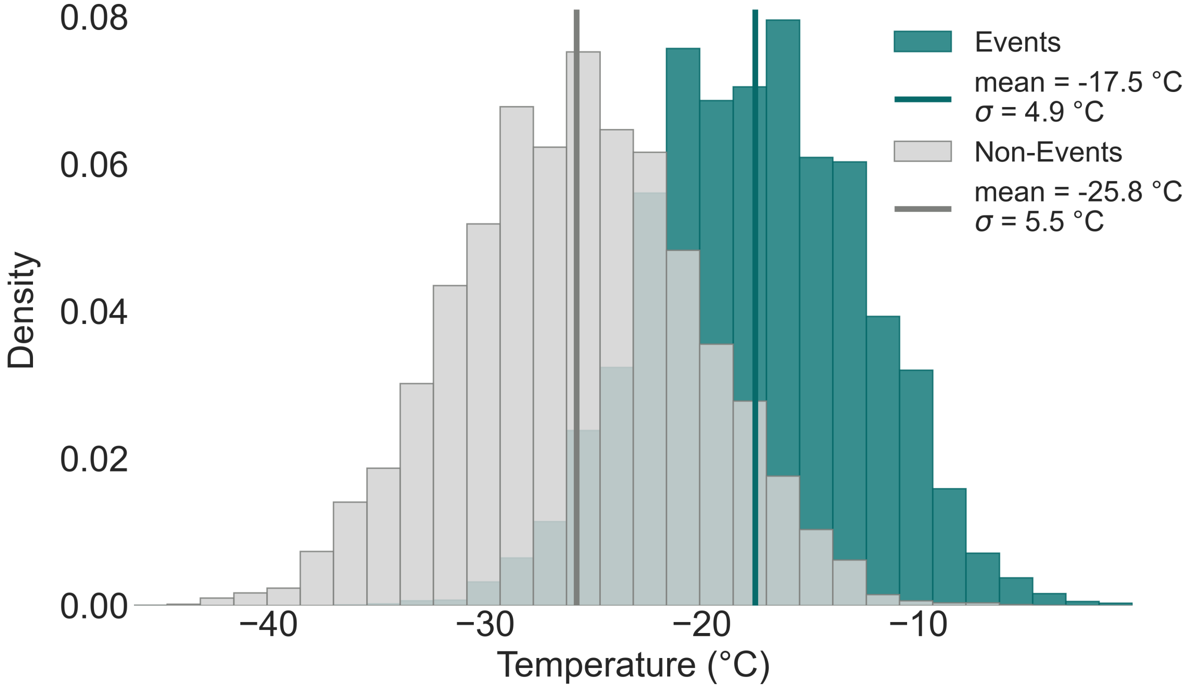

Figure 8. Histogram of Marble Point 10-minute temperature measurements from April–August, 2013–2024, for events (green) and non-events (grey). Here, an event corresponds to a breakout event as defined in Sect. 2.1 (FIBEs and POs). The vertical lines in green and grey indicate the means of the individual distributions. The mean and standard deviation of each distribution is stated in the legend.

a higher SLP on the East Antarctic Ice Sheet. The resulting pressure gradient is perpendicular to the red band of trajectories, forcing a geostrophic response along the Transantarctic Mountains, typical for the Ross Ice Shelf airstream (O'Connor et al., 1994; Parish et al., 2006).

To better understand the difference in environments during events and non-events, the difference in wind speed, 2-m temperature and SLP composites for events and non-events is shown in Fig. 11. Wind speed and 2-m temperature over the Ross Sea are consistently higher during breakout events than non-events. These regions of higher wind speed and higher temperature lie to the south-west of the negative SLP anomaly in the Ross Sea during outbreak events. The location of the anomalous wind speed and temperature demonstrates the important role of the SLP in the Ross Sea, that leads to favourable conditions for the advection of warm air towards McMurdo Sound and simultaneously to the evolution of barrier winds along the Transantarctic Mountains. The patterns observed in the trajectories (Fig. 10), as well as wind, temperature and SLP anomalies on the Ross Ice Shelf (Fig. 11) connect the strong winds in McMurdo Sound during sea ice breakout events to the barrier wind regime known as the Ross Ice Shelf airstream (Parish et al., 2006; Seefeldt and Cassano, 2012), which is characterised by positive temperature anomalies on the Ross Ice Shelf, a strong pressure gradient perpendicular to the Transantarctic Mountains and strong winds along the the Transantarctic Mountains (Parish et al., 2006; Seefeldt and Cassano, 2012; Chenoli et al., 2013; Coggins et al.,

https://doi.org/10.5194/egusphere-2026-4721
Preprint. Discussion started: 22 September 2026

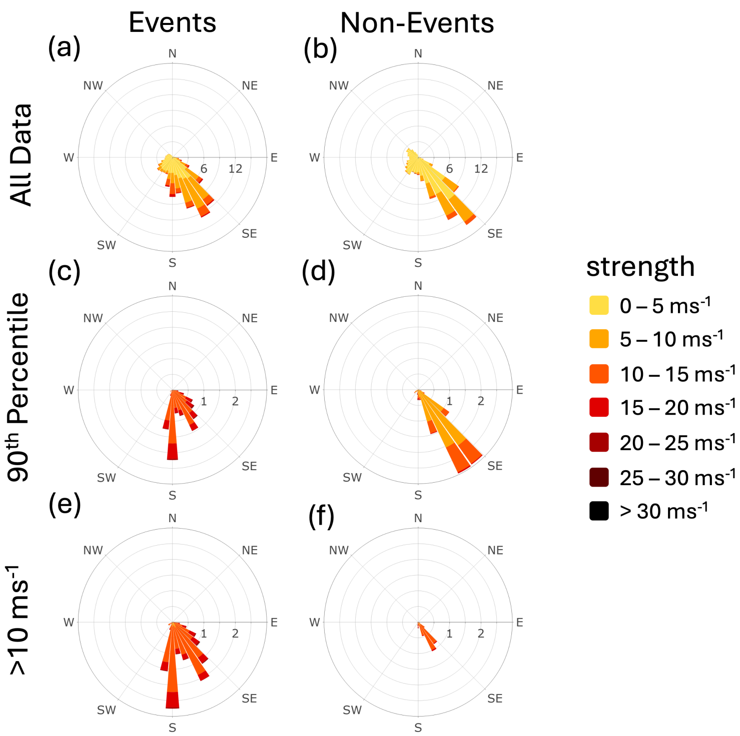

Figure 9. Wind roses constructed from Marble Point 10-minute wind measurements from April–August, 2013–2024, for breakout events (left column) and non-breakout events (right column). The first row shows the full data sets, the second row shows wind speeds above the 2013–2024 90th percentile of each category ($10.8\,\mathrm{m\,s^{-1}}$ for events and $7.4\,\mathrm{m\,s^{-1}}$ for non-events), and the third row shows wind speeds above $10\,\mathrm{m\,s^{-1}}$. The maximum frequency in the first row is 18 %, with each circle representing an increment of 3 %. The maximum frequency in the other two rows is 3 %, with each circle representing an increment of 0.5 %. The wind direction is defined as the bearing from which the wind originated. The bin size of each spoke is 10°.

2014; Costanza et al., 2016). During a typical Ross Ice Shelf airstream event there are two wind speed maxima: one east of Ross Island and one where the Amundsen Coast meets the Ross Ice Shelf (Parish et al., 2006; Coggins et al., 2014). We observe three positive wind speed anomalies during outbreak events: one where the Amundsen Coast meets the Ross Ice Shelf and one each east and west of Ross Island respectively: (Fig. 11a, the three red regions). The location of the maximum at the Amundsen Coast lies on the grounding line and is probably caused by the slope of the West Antarctic Ice Sheet onto the Ross Ice Shelf. The location of two maxima around Ross Island coincides with the polynya in McMurdo Sound (west of the Island), and the Ross Sea Polynya (large red area east of Ross island in Fig. 11a). While our focus in this paper was the McMurdo Sound polynya, it is noteworthy that in Antarctica, the highest coastal sea ice production occurs in the three polynyas of the Ross Ice Shelf Polynya region, of which the Ross Sea Polynya has the largest area (Tamura et al., 2008; Burada et al., 2023). Dale et al. (2017) already showed that strong winds are linked to sea ice breakout events in the Ross Sea Polynya, and our results indicate

https://doi.org/10.5194/egusphere-2026-4721
Preprint. Discussion started: 22 September 2026

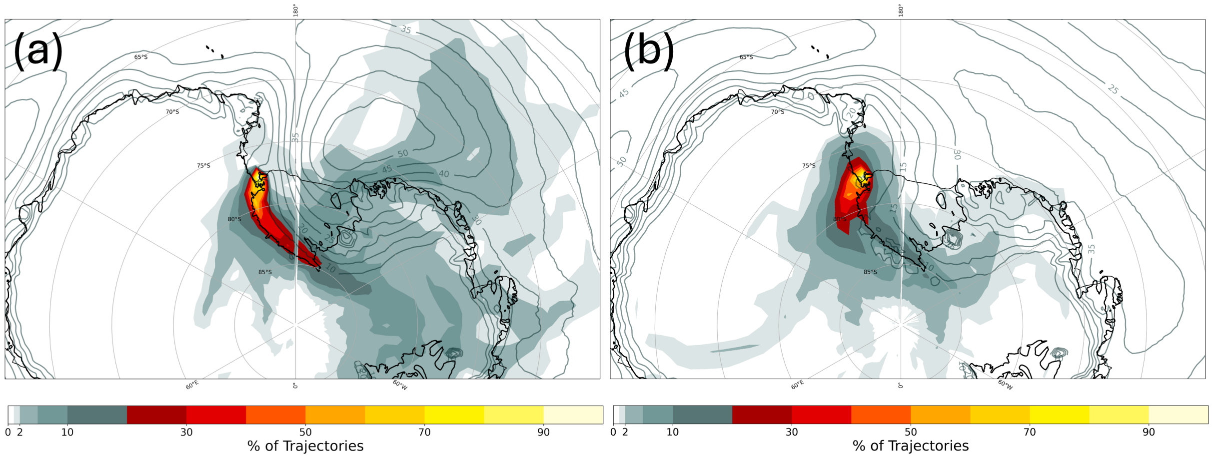

Figure 10. Pathways of the 4-day backward trajectories from McMurdo Sound during **(a)** breakout events and **(b)** non-events in April–August, 2013–2024. The thin black line outlines the Antarctic continent. Gray lines show cyclone frequency contours (every 5 %). Colours indicate the percentage of trajectories that crossed a 1° × 4° grid box.

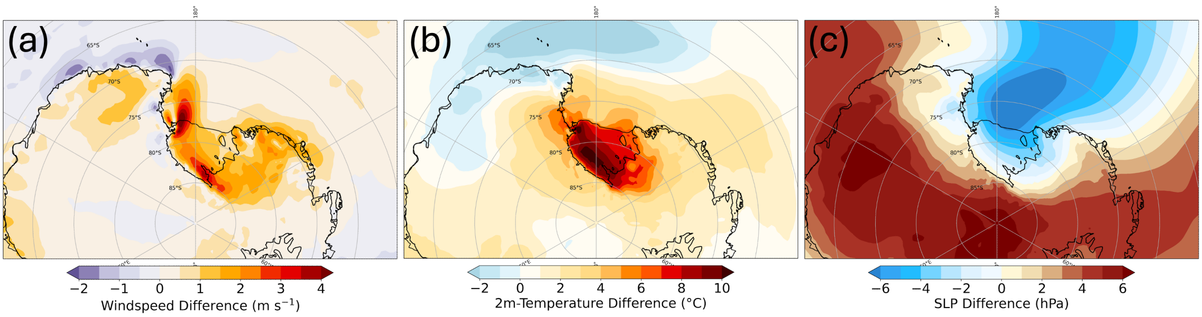

Figure 11. Composite differences between events and non-events of the ERA5 fields **(a)** 10-m wind speed, **(b)** 2-m temperature, and **(c)** SLP. Positive values indicate higher values during events compared to non-events.

that the same conditions that affect the McMurdo Sound polynya (Ross Ice Shelf airstream leading to high winds and high temperatures in certain regions), likely lead to breakouts and polynya openings in the much larger Ross Sea Polynya.

3.4 Cyclone frequency

The previous section identified that the Ross Ice Shelf airstream is important in directing air parcels towards the McMurdo Sound, leading to strong winds and sea ice breakout events in McMurdo Sound. Since the evolution of the Ross Ice Shelf airstream is modulated by the SLP field (via the geostrophic wind relationship), which in turn is strongly influenced by the presence of extratropical cyclones in the Ross Sea, this section discusses some characteristics of the cyclones linked to breakout events in McMurdo Sound.

https://doi.org/10.5194/egusphere-2026-4721
Preprint. Discussion started: 22 September 2026

To quantify the importance of cyclones in the Ross Sea for breakout events in McMurdo Sound, the spatial mean in the winter (April–August) cyclone frequency in the Ross Sea region (see Sect. 2.3.2) is compared to the annual number of breakout events from 2013–2024 (Fig. 5b). The correlation between the winter-mean cyclone frequency and the number of breakout events in McMurdo Sound is high, as quantified by a Pearson correlation coefficient of 0.83 and a Spearman correlation coefficient of 0.80. This clearly reveals the importance of the Southern Ocean storm track dynamics for the sea ice variability in McMurdo Sound. It is, however, important to note that due to the relatively large distance between the Ross Sea cyclones and McMurdo Sound, these cyclones lead to sea ice breakout events *indirectly*, i.e. they induce a Ross Ice Shelf airstream, which leads to strong winds in McMurdo Sound, and eventually to the breakout of sea ice in McMurdo Sound. This is in contrast to other regions in Antarctica, both in the Marginal Ice Zone and at other coastal polynyas, where cyclones directly influence sea ice variability through the surface winds associated with these weather systems (Heil, 2006; Schemm, 2018; Zhong et al., 2025). Frequent FIBEs were observed in the winters 2019, 2022, 2024 (Fig. 4), the same years in which the fast ice cover was considered too unstable for conducting station operations. The FIBEs lasted unusually late into the winter, as late as mid-July to mid-August. As in all other years considered, they coincided with strong southerly winds and positive temperature anomalies (Fig. 7). From Fig. 5b we see that in the years when the stable fast ice cover formed unusually late (2019, 2022, 2024) there is a higher cyclone frequency in the eastern Ross Sea, and there are more southerly strong wind events.

Not every cyclone passing through the Ross Sea leads to a breakout event in McMurdo Sound, raising the question if cyclones linked to breakout events have any specific characteristics. Figure 12 shows a histogram of the minimum SLP within cyclones in the sector indicated in Fig. 3 at times that coincide with breakout events in McMurdo Sound (events) and times that do not (non-events). Minimum SLP is an often used measure for cyclone intensity (e.g., Wernli and Schwierz, 2006). There is a difference of 4.4 hPa in the mean cyclone intensity during events and non-events (Fig. 12). This difference does not exceed the 1σ-range, but there is a clear shift in the intensity distribution, indicating that there are deeper cyclones in the Ross Sea during breakout events than during periods without breakout events. Deeper cyclones during outbreak events lead to stronger negative SLP anomalies in the Ross Sea (Fig. 11), thus linking the cyclones in the Ross Sea to the SLP anomalies across the region that induce barrier winds along the Transantarctic Mountains.

4 Conclusions

This study contributes to the understanding of the synoptic atmospheric processes that govern winter sea ice variability in McMurdo Sound during a 12-year period. Spatially averaged sea ice concentration data were used to identify breakout events in McMurdo Sound, categorising them as fast ice breakout events (FIBEs) or polynya openings (POs), depending on the latitude of the ice edge (Fig. 4). Wind and temperature measurements from Marble Point were used to connect sea ice variability and local meteorological conditions in McMurdo Sound to large-scale atmospheric fields of wind, temperature and SLP in the Ross Sea area. The large-scale atmospheric flow leading up to breakout events was analysed with Lagrangian backward trajectories, a composite approach, and an objective cyclone identification based on ERA5 reanalysis data.

Our study led to the following four key findings.

https://doi.org/10.5194/egusphere-2026-4721
Preprint. Discussion started: 22 September 2026

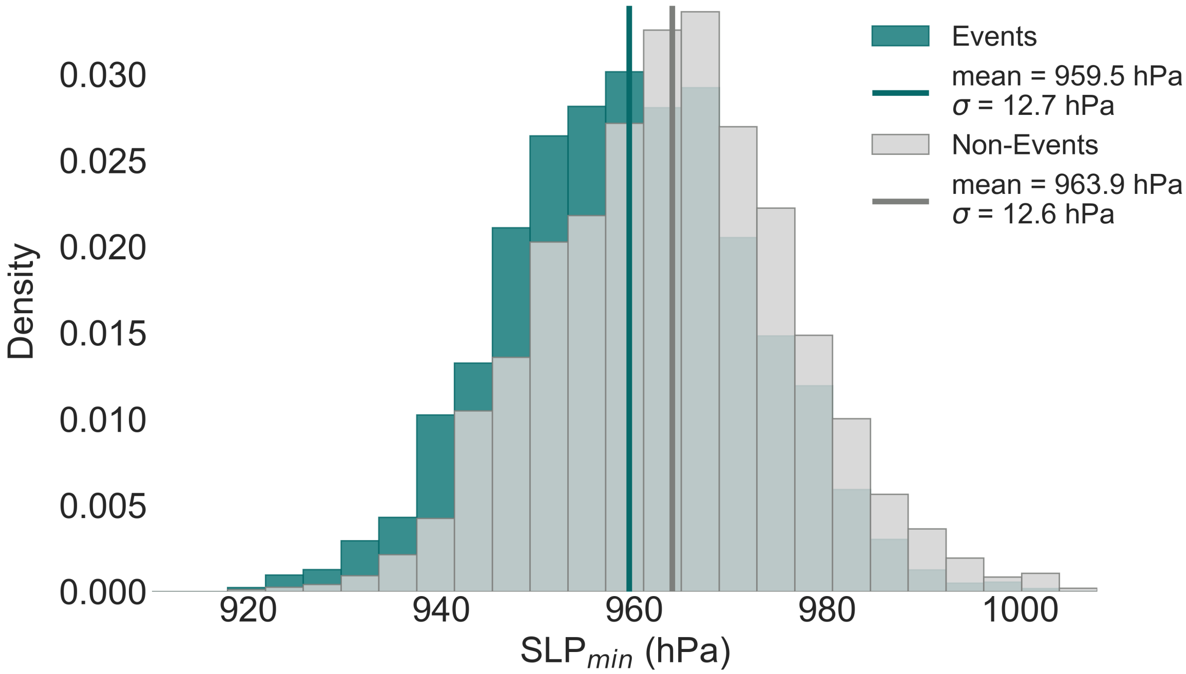

Figure 12. Histogram of minimum SLP associated with cyclones in the Ross Sea region (Fig. 3) in the winter seasons (April–August), 2013–2024, for McMurdo Sound breakout events (green) and non-events (grey). The vertical lines indicate the means of the distributions. The standard deviation of each distribution is stated in the legend.

1. **In the 12 year record, there is no statistically significant trend in the sum of FIBEs and POs but there is a regime shift from mostly POs to FIBEs.** Our results show strong evidence that the atmosphere is the key driver of the overall number of breakout events in the years we considered (Fig. 5b). The increasing prevalence of FIBEs since 2019 implies that winter polynyas in McMurdo Sound have become larger, consistent with recent observations of an increasing coastal polynya area in the Ross Sea and around Antarctica (Duffy et al., 2024; Yang et al., 2025). This demonstrates that the distinction between POs and FIBEs captures a meaningful change in the sea ice variability of McMurdo Sound. However, from a synoptic perspective, it remains unclear why the breakout events are mostly POs from 2013–2018 and FIBEs from 2019–2024. Further research into other contributing factors, such as atmospheric or oceanic preconditioning (e.g. tides or warm currents; Wei et al., 2021), is required to fully understand why the fast ice took so long to form a stable cover in certain years with frequent FIBEs.

2. **Breakout events in McMurdo Sound are associated with strong southerly winds and positive temperature anomalies.** Our results show that both FIBEs and POs consistently coincide with strong southerly winds (typically >10 $m\,s^{-1}$) at Marble Point, confirming previous studies that identified wind as the primary driver of fast ice breakup. In addition, we demonstrate that these events are systematically accompanied by positive 2-m temperature anomalies, often exceeding

https://doi.org/10.5194/egusphere-2026-4721
Preprint. Discussion started: 22 September 2026

the climatological 90th percentile. Although air temperatures remain well below freezing and therefore cannot directly melt the sea ice, these warm anomalies are likely to influence the rate of sea ice formation following a breakout by reducing thermodynamic ice growth. This previously unreported direct link between breakout events and large scale warm air anomalies provides a new perspective on the atmospheric conditions accompanying winter polynya activity in McMurdo Sound.

3. **Breakout events are associated with the Ross Ice Shelf airstream.** Backward trajectories show that air parcels associated with the identified breakout events are advected rapidly along the Transantarctic Mountains toward McMurdo Sound, driven by an enhanced pressure gradient between the Antarctic continent and the Ross Sea (Fig. 11c). The wind anomaly pattern during breakout events (Fig. 11a) shows clear signatures of the Ross Ice Shelf airstream, in good agreement with the literature (e.g., Parish et al., 2006; Seefeldt and Cassano, 2012). While the Ross Ice Shelf airstream has previously been recognised as an important component of the regional circulation, this study provides the first direct link between this atmospheric flow regime and winter sea ice breakout events in McMurdo Sound.

4. **Cyclones influence breakout events indirectly.** An analysis of the large-scale atmospheric flow leading up to sea ice breakout events in McMurdo Sound revealed that approximately 80% of the variability in the annual number of wintertime breakout events in McMurdo Sound can be explained by the variability in cyclone frequency in the Ross Sea. No previous studies investigated the relationship between Ross Sea cyclone frequency and the number of breakout events in McMurdo Sound. The cyclones occurring during breakout events tend to be deeper than those during non-event periods. This results in a stronger pressure gradient, which drives the Ross Ice Shelf airstream, thereby linking cyclone activity to local wind conditions in McMurdo Sound. Unlike many Antarctic coastal regions, where cyclones directly affect the sea ice through their surface winds, our results indicate that cyclones influence McMurdo Sound indirectly through their control of the large-scale circulation. This indirect pathway represents an important new contribution to our understanding of atmosphere-sea ice interactions in the Ross Sea sector.

Overall, our results suggest a chain of processes linking synoptic-scale atmospheric variability to local sea ice conditions: enhanced cyclone activity in the Ross Sea favours the development of the Ross Ice Shelf airstream, which transports relatively warm air and generates strong southerly winds in McMurdo Sound, also influenced by local topography, ultimately causing mechanical breakup of the fast ice. Future changes in the Ross Sea atmosphere may substantially influence the stability of fast ice in McMurdo Sound. Climate model projections generally indicate a poleward shift and intensification of Southern Hemisphere storm tracks (e.g., Yin, 2005; O'Gorman, 2010), accompanied by changes in the frequency and intensity of Ross Sea storms (O'Gorman, 2010; Radlwimmer et al., 2026). Although considerable uncertainty remains regarding regional cyclone trends, our results indicate that an increase in strong cyclones or more frequent Ross Ice Shelf airstream events would favour more frequent winter fast ice break-outs and larger coastal polynyas. At the same time, a warmer atmosphere could reduce the rate at which newly opened polynyas refreeze, reinforcing the impact of mechanically driven breakout events. Such changes would have important implications for the regional sea ice cover, ocean-atmosphere heat exchange, sea ice production, and Antarctic Bottom Water formation.

https://doi.org/10.5194/egusphere-2026-4721
Preprint. Discussion started: 22 September 2026

Data availability. Marble Point weather station data are available from https://amrdcdata.ssec.wisc.edu/ (last access: 1 July 2025). ARTIST sea-ice concentration data can be accessed from the University of Bremen data archive at https://seaice.uni-bremen.de/data-archive/ (last accessed: 1 July 2025) (Spreen et al., 2008). ERA5 data are openly available on the Copernicus Climate Change Service (C3S) Climate Data Store at https://doi.org/10.24381/cds.bd0915c6 (Hersbach et al., 2020).

https://doi.org/10.5194/egusphere-2026-4721
Preprint. Discussion started: 22 September 2026

Appendix A

Table A1. Dates of sea ice breakout events and non-event dates in McMurdo Sound, identified with the approach listed in Sect. 2.1, as well as the total number of days per year of events (Nr E-Days) and non-events (Nr N-Days). Bold event dates indicate FIBEs.

Year	Event Dates	Nr E-Days	Non-Event Dates	Nr N-Days
2013	**14.4–18.4**, **29.4–5.5**, **16.5–31.5**, 9.6–26.6	46	1.4–14.4, 18.4–29.4, 5.5–16.5, 31.5–9.6, 26.6–31.8	115
2014	4.5–15.5, 30.5–5.6, 20.7–23.7, 5.8–23.8, 25.8–31.8	49	20.4–4.5, 15.5–30.5, 5.6–20.7, 23.7–5.8, 23.8–25.8	94
2015	21.4–27.4, 1.6–11.6, 12.6–14.6, 20.8–23.8, 25.8–31.8	32	1.4–21.4, 27.4–1.6, 11.6–12.6, 14.6–20.8, 23.8–25.8	130
2016	8.4–12.4, 18.4–25.4, 24.5–28.5, 1.6–3.6	21	4.4–8.4, 12.4–18.4, 25.4–24.5, 28.5–1.6, 3.6–31.8	137
2017	27.4–30.4, 2.5–11.5, 15.5–28.5, 31.5–20.6, 20.7–29.7, 13.8–27.8	74	9.4–27.4, 30.4–2.5, 11.5–15.5, 28.5–31.5, 20.6–20.7, 29.7–13.8, 27.8–31.8	83
2018	**25.4–5.5**, **13.5–18.5**, 7.6–13.6, 15.6–23.6, 20.7–28.7, 13.8–18.8	48	10.4–25.4, 5.5–13.5, 18.5–7.6, 13.6–15.6, 23.6–20.7, 28.7–13.8, 18.8–31.8	108
2019	**17.4–22.4**, **23.4–27.4**, **1.5–8.5**, **9.5–31.5**, **9.6–15.6**, **25.6–2.7**, **6.7–14.7**, 11.8–30.8	86	1.4–17.4, 22.4–23.4, 27.4–1.5, 8.5–9.5, 31.5–9.6, 15.6–25.6, 2.7–6.7, 14.7–11.8, 30.8–31.8	83
2020	**8.4–17.4**, **19.4–27.4**, **30.5–4.6**, 9.6–11.6, **20.6–6.7**, **10.7–17.7**, **24.7–28.7**, **9.8–31.8**	81	2.4–8.4, 17.4–19.4, 27.4–30.5, 4.6–9.6, 11.6–20.6, 6.7–10.7, 17.7–24.7, 28.7–9.8	86
2021	**26.4–28.4**, **3.5–5.5**, **6.5–9.5**, 25.5–31.5, 3.7–11.7, 21.7–25.7	31	10.4–26.4, 28.4–3.5, 5.5–6.5, 9.5–25.5, 31.5–3.7, 11.7–21.7, 25.7–31.8	125
2022	**1.4–6.4**, **13.4–18.4**, **24.4–30.4**, **11.5–5.6**, **6.6–18.6**, **1.7–7.7**, **19.7–23.7**, **26.7–18.8**	94	6.4–13.4, 18.4–24.4, 30.4–11.5, 5.6–6.6, 18.6–1.7, 7.7–19.7, 23.7–26.7, 18.8–31.8	74
2023	**20.4–29.4**, **1.5–5.5**, **5.6–17.6**	28	1.4–20.4, 29.4–1.5, 5.5–5.6, 17.6–31.8	131
2024	**13.4–23.4**, **27.4–30.4**, **3.5–10.5**, **31.5–4.6**, **5.6–19.6**, **30.6–3.7**, **17.7–21.7**, **31.7–19.8**	72	9.4–13.4, 23.4–27.4, 30.4–3.5, 10.5–31.5, 4.6–5.6, 19.6–30.6, 3.7–17.7, 21.7–31.7, 19.8–31.8	89
Total		**662**		**1259**

Author contributions. This paper is an outcome of MF's MSc thesis, supervised by RD and HW. MF performed all the analyses and wrote the first version of the paper. All co-authors supported the interpretation of the results and contributed to the writing.

Competing interests. The authors declare that they have no conflict of interest.

Acknowledgements. This work has been supported by the Antarctic Sea-Ice Switch Programme (contract: RTVU2448) funded by the New Zealand Ministry for Business, Innovation and Employment (MBIE). The authors appreciate the support of the University of Wisconsin-Madison and Madison College AMRDC for the data set, data display, and information, NSF grant number 1951720 (UW) and 1951603 (MATC). We thank Gunnar Spreen from the Institute of Environmental Physics, University of Bremen for the provision of the AMSR2 sea-ice concentration data. We acknowledge the use of imagery from the Worldview Snapshots application (https://wvs.earthdata.nasa.gov), part of the Earth Science Data and Information System (ESDIS). The authors are very grateful to Petra Heil, Greg Leonard, and David Mikolajczyk for their insightful input which shaped the project at its beginning stages. The AI tool ChatGPT−5.6 (OpenAI) was used for a first draft of the conclusion. After using this tool, the authors reviewed and edited the draft as needed and take full responsibility for the content of this manuscript.

https://doi.org/10.5194/egusphere-2026-4721
Preprint. Discussion started: 22 September 2026

References

Antarctic Meteorological Research and Data Center: Marble Point Automatic Weather Station, 2024 quality-controlled observational data. AMRDC Data Repository, https://doi.org/10.48567/YMVA-WE33, accessed: 2026-07-23., 2024.

Arrigo, K. R. and Van Dijken, G. L.: Phytoplankton dynamics within 37 Antarctic coastal polynya systems, J. Geophys. Res., 108, 3271, https://doi.org/10.1029/2002JC001739, 2003.

Burada, G. K., McDonald, A., Renwick, J., and Jolly, B.: Delineating polynya area using active and passive microwave sensors for the Western Ross Sea Sector of Antarctica, Remote Sens., 15, 2545, https://doi.org/10.3390/rs15102545, 2023.

Chenoli, S. N., Turner, J., and Samah, A. A.: A climatology of strong wind events at McMurdo station, Antarctica, Int. J. Climatol., 33, 2667–2681, https://doi.org/10.1002/joc.3617, 2013.

Coggins, J. H. J., McDonald, A. J., and Jolly, B.: Synoptic climatology of the Ross Ice Shelf and Ross Sea region of Antarctica: k -means clustering and validation, Int. J. Climatol., 34, 2330–2348, https://doi.org/10.1002/joc.3842, 2014.

Costanza, C. A., Lazzara, M. A., Keller, L. M., and Cassano, J. J.: The surface climatology of the Ross Ice Shelf Antarctica, Int. J. Climatol., 36, 4929–4941, https://doi.org/10.1002/joc.4681, 2016.

Dale, E. R., McDonald, A. J., Coggins, J. H. J., and Rack, W.: Atmospheric forcing of sea ice anomalies in the Ross Sea polynya region, Cryosphere, 11, 267–280, https://doi.org/10.5194/tc-11-267-2017, 2017.

Duffy, G. A., Montiel, F., Purich, A., and Fraser, C. I.: Emerging long-term trends and interdecadal cycles in Antarctic polynyas, Proc. Natl. Acad. Sci. U.S.A., 121, e2321595 121, https://doi.org/10.1073/pnas.2321595121, 2024.

Eayrs, C., Li, X., Raphael, M. N., and Holland, D. M.: Rapid decline in Antarctic sea ice in recent years hints at future change, Nat. Geosci., 14, 460–464, https://doi.org/10.1038/s41561-021-00768-3, 2021.

Fonseca, R., Francis, D., Aulicino, G., Mattingly, K. S., Fusco, G., and Budillon, G.: Atmospheric controls on the Terra Nova Bay polynya occurrence in Antarctica, Clim. Dyn., 61, 5147–5169, https://doi.org/10.1007/s00382-023-06845-0, 2023.

Fraser, A. D., Ohshima, K. I., Nihashi, S., Massom, R. A., Tamura, T., Nakata, K., Williams, G. D., Carpentier, S., and Willmes, S.: Landfast ice controls on sea-ice production in the Cape Darnley Polynya: A case study, Remote Sens. Environ., 233, 111 315, https://doi.org/10.1016/j.rse.2019.111315, 2019.

Fraser, A. D., Wongpan, P., Langhorne, P. J., Klekociuk, A. R., Kusahara, K., Lannuzel, D., Massom, R. A., Meiners, K. M., Swadling, K. M., Atwater, D. P., Brett, G. M., Corkill, M., Dalman, L. A., Fiddes, S., Granata, A., Guglielmo, L., Heil, P., Leonard, G. H., Mahoney, A. R., McMinn, A., van der Merwe, P., Weldrick, C. K., and Wienecke, B.: Antarctic landfast sea ice: A review of its physics, biogeochemistry and ecology, Rev. Geophys., 61, e2022RG000 770, https://doi.org/10.1029/2022RG000770, 2023.

Golledge, N. R., Keller, E. D., Gossart, A., Malyarenko, A., Bahamondes-Dominguez, A., Krapp, M., Jendersie, S., Lowry, D. P., Alevropoulos-Borrill, A., and Notz, D.: Antarctic coastal polynyas in the global climate system, Nat. Rev. Earth Environ., 6, 126–139, https://doi.org/10.1038/s43017-024-00634-x, 2025.

Heil, P.: Atmospheric conditions and fast ice at Davis, East Antarctica: A case study, J. Geophys. Res., 111, C05 009, https://doi.org/10.1029/2005JC002904, 2006.

Hersbach, H., Bell, B., Berrisford, P., Hirahara, S., Horányi, A., Muñoz-Sabater, J., Nicolas, J., Peubey, C., Radu, R., Schepers, D., Simmons, A., Soci, C., Abdalla, S., Abellan, X., Balsamo, G., Bechtold, P., Biavati, G., Bidlot, J., Bonavita, M., De Chiara, G., Dahlgren, P., Dee, D., Diamantakis, M., Dragani, R., Flemming, J., Forbes, R., Fuentes, M., Geer, A., Haimberger, L., Healy, S., Hogan, R. J., Hólm, E.,

https://doi.org/10.5194/egusphere-2026-4721
Preprint. Discussion started: 22 September 2026

Janisková, M., Keeley, S., Laloyaux, P., Lopez, P., Lupu, C., Radnoti, G., De Rosnay, P., Rozum, I., Vamborg, F., Villaume, S., and Thépaut, J.: The ERA5 global reanalysis, Q. J. R. Meteorol. Soc., 146, 1999–2049, https://doi.org/10.1002/qj.3803, 2020.

Holland, M. M., Landrum, L., Raphael, M., and Stammerjohn, S.: Springtime winds drive Ross Sea ice variability and change in the following autumn, Nat. Commun., 8, 731, https://doi.org/10.1038/s41467-017-00820-0, 2017.

Huot, P.-V., Kittel, C., Fichefet, T., Jourdain, N. C., Sterlin, J., and Fettweis, X.: Effects of the atmospheric forcing resolution on simulated sea ice and polynyas off Adélie Land, East Antarctica, Ocean Modell., 168, 101 901, https://doi.org/10.1016/j.ocemod.2021.101901, 2021.

Jacobs, S. S.: Bottom water production and its links with the thermohaline circulation, Antarct. Sci., 16, 427–437, https://doi.org/10.1017/S095410200400224X, 2004.

Kim, S., Saenz, B., Scanniello, J., Daly, K., and Ainley, D.: Local climatology of fast ice in McMurdo Sound, Antarctica, Antarct. Sci., 30, 125–142, https://doi.org/10.1017/S0954102017000578, 2018.

Langhorne, P. J., Haas, C., Price, D., Rack, W., Leonard, G. H., Brett, G. M., and Urbini, S.: Fast ice thickness distribution in the western Ross Sea in late spring, J. Geophys. Res., 128, e2022JC019 459, https://doi.org/10.1029/2022JC019459, 2023.

Leonard, G. H., Turner, K. E., Richter, M. E., Whittaker, M. S., and Smith, I. J.: Brief communication: The anomalous winter 2019 sea-ice conditions in McMurdo Sound, Antarctica, Cryosphere, 15, 4999–5006, https://doi.org/10.5194/tc-15-4999-2021, 2021.

Massom, R. A., Hill, K. L., Lytle, V. I., Worby, A. P., Paget, M., and Allison, I.: Effects of regional fast-ice and iceberg distributions on the behaviour of the Mertz Glacier polynya, East Antarctica, Ann. Glaciol., 33, 391–398, https://doi.org/10.3189/172756401781818518, 2001.

Meehl, G. A., Arblaster, J. M., Chung, C. T. Y., Holland, M. M., DuVivier, A., Thompson, L., Yang, D., and Bitz, C. M.: Sustained ocean changes contributed to sudden Antarctic sea ice retreat in late 2016, Nat. Commun., 10, 14, https://doi.org/10.1038/s41467-018-07865-9, 2019.

NASA Worldview Snapshots: Ross Sea, Antarctica (Morning Overpass), MODIS https://worldview.earthdata.nasa.gov/?v=-241184.9654588122,-1633471.5079556804,894498.5581855325,-1073207.938076832&r=168.286&p=antarctic&t=2007-12-12-T06%3A32%3A32Z. accessed 03-08-2026, 2007.

National Snow and Ice Data Center: Sea Ice | National Snow and Ice Data Center, https://nsidc.org/learn/parts-cryosphere/sea-ice, 2024.

Nihashi, S. and Ohshima, K. I.: Circumpolar mapping of Antarctic coastal polynyas and landfast sea ice: relationship and variability, J. Climate, 28, 3650–3670, https://doi.org/10.1175/JCLI-D-14-00369.1, 2015.

O'Connor, W. P. and Bromwich, D. H.: Surface airflow around Windless Bight, Ross Island, Antarctica, Q. J. R. Meteorol. Soc., 114, 917–938, https://doi.org/10.1002/qj.49711448205, 1988.

O'Connor, W. P., Bromwich, D. H., and Carrasco, J. F.: Cyclonically forced barrier winds along the Transantarctic Mountains near Ross Island, Mon. Wea. Rev., 122, 137–150, https://doi.org/10.1175/1520-0493(1994)122<0137:CFBWAT>2.0.CO;2, 1994.

O'Gorman, P. A.: Understanding the varied response of the extratropical storm tracks to climate change, Proc. Natl. Acad. Sci. U.S.A., 107, 19 176–19 180, https://doi.org/10.1073/pnas.1011547107, 2010.

Papritz, L., Pfahl, S., Rudeva, I., Simmonds, I., Sodemann, H., and Wernli, H.: The Role of Extratropical Cyclones and Fronts for Southern Ocean Freshwater Fluxes, J. Climate, 27, 6205–6224, https://doi.org/10.1175/JCLI-D-13-00409.1, 2014.

Parish, T. R., Cassano, J. J., and Seefeldt, M. W.: Characteristics of the Ross Ice Shelf air stream as depicted in Antarctic Mesoscale Prediction System simulations, J. Geophys. Res., 111, 2005JD006 185, https://doi.org/10.1029/2005JD006185, 2006.

Parkinson, C. L.: A 40-y record reveals gradual Antarctic sea ice increases followed by decreases at rates far exceeding the rates seen in the Arctic, Proc. Natl. Acad. Sci. U.S.A., 116, 14 414–14 423, https://doi.org/10.1073/pnas.1906556116, 2019.

https://doi.org/10.5194/egusphere-2026-4721
Preprint. Discussion started: 22 September 2026

Pistone, K., Eisenman, I., and Ramanathan, V.: Observational determination of albedo decrease caused by vanishing Arctic sea ice, Proc. Natl. Acad. Sci. U.S.A., 111, 3322–3326, https://doi.org/10.1073/pnas.1318201111, 2014.

Price, D.: Assessment of Antarctic sea ice by surface validated satellite measurements, PhD Thesis, University of Canterbury, https://doi.org/10.13140/RG.2.2.25248.10248, 2014.

Radlwimmer, A. L., Leonard, G. H., Pauling, A. G., Smith, I. J., and Montiel, F.: Increasing Winter Storminess in the Southern Ross Sea, Antarctica, and Its Impact on Land-Fast Sea-Ice, Geophys. Res. Lett., 53, e2026GL123 090, https://doi.org/10.1029/2026GL123090, 2026.

Richter, M. E., Leonard, G. H., Smith, I. J., Langhorne, P. J., and Parry, M.: The Interannual Variability of Antarctic Fast-Ice Thickness in McMurdo Sound and Connections to Climate, J. Geophys. Res., 129, e2023JC020 134, https://doi.org/10.1029/2023JC020134, 2024.

Roach, L. A. and Meier, W. N.: Sea ice in 2023, Nat. Rev. Earth Environ., 5, 235–237, https://doi.org/10.1038/s43017-024-00542-0, 2024.

Schemm, S.: Regional Trends in Weather Systems Help Explain Antarctic Sea Ice Trends, Geophys. Res. Lett., 45, 7165–7175, https://doi.org/10.1029/2018GL079109, 2018.

Schlosser, E., Haumann, F. A., and Raphael, M. N.: Atmospheric influences on the anomalous 2016 Antarctic sea ice decay, Cryosphere, 12, 1103–1119, https://doi.org/10.5194/tc-12-1103-2018, 2018.

Seefeldt, M. W. and Cassano, J. J.: A description of the Ross Ice Shelf air stream (RAS) through the use of self-organizing maps (SOMs), J. Geophys. Res., 117, 2011JD016 857, https://doi.org/10.1029/2011JD016857, 2012.

Seefeldt, M. W., Tripoli, G. J., and Stearns, C. R.: A High-Resolution Numerical Simulation of the Wind Flow in the Ross Island Region, Antarctica, Mon. Wea. Rev., 131, 435–458, https://doi.org/10.1175/1520-0493(2003)131<0435:AHRNSO>2.0.CO;2, 2003.

Spreen, G., Kaleschke, L., and Heygster, G.: Sea ice remote sensing using AMSR-E 89-GHz channels, J. Geophys. Res., 113, 2005JC003 384, https://doi.org/10.1029/2005JC003384, 2008.

Sprenger, M. and Wernli, H.: The LAGRANTO Lagrangian analysis tool – version 2.0, Geosci. Model Dev., 8, 2569–2586, https://doi.org/10.5194/gmd-8-2569-2015, 2015.

Sprenger, M., Fragkoulidis, G., Binder, H., Croci-Maspoli, M., Graf, P., Grams, C. M., Knippertz, P., Madonna, E., Schemm, S., Škerlak, B., and Wernli, H.: Global Climatologies of Eulerian and Lagrangian Flow Features based on ERA-Interim, Bull. Am. Meteorol. Soc., 98, 1739–1748, https://doi.org/10.1175/BAMS-D-15-00299.1, 2017.

Stefan, J.: Ueber die Theorie der Eisbildung, insbesondere über die Eisbildung im Polarmeere, Ann. Phys., 278, 269–286, https://doi.org/10.1002/andp.18912780206, 1891.

Stuecker, M. F., Bitz, C. M., and Armour, K. C.: Conditions leading to the unprecedented low Antarctic sea ice extent during the 2016 austral spring season, Geophys. Res. Lett., 44, 9008–9019, https://doi.org/10.1002/2017GL074691, 2017.

Stössel, A., Yang, K., and Kim, S.-J.: On the Role of Sea Ice and Convection in a Global Ocean Model, J. Phys. Oceanogr., 32, 1194–1208, https://doi.org/10.1175/1520-0485(2002)032<1194:OTROSI>2.0.CO;2, 2002.

Tamura, T., Ohshima, K. I., and Nihashi, S.: Mapping of sea ice production for Antarctic coastal polynyas, Geophys. Res. Lett., 35, L07 606, https://doi.org/10.1029/2007GL032903, 2008.

Tamura, T., Ohshima, K. I., Fraser, A. D., and Williams, G. D.: Sea ice production variability in Antarctic coastal polynyas, J. Geophys. Res., 121, 2967–2979, https://doi.org/10.1002/2015JC011537, 2016.

Turner, J., Phillips, T., Marshall, G. J., Hosking, J. S., Pope, J. O., Bracegirdle, T. J., and Deb, P.: Unprecedented springtime retreat of Antarctic sea ice in 2016, Geophys. Res. Lett., 44, 6868–6875, https://doi.org/10.1002/2017GL073656, 2017.

Wang, G., Hendon, H. H., Arblaster, J. M., Lim, E.-P., Abhik, S., and Van Rensch, P.: Compounding tropical and stratospheric forcing of the record low Antarctic sea-ice in 2016, Nat. Commun., 10, 13, https://doi.org/10.1038/s41467-018-07689-7, 2019.

https://doi.org/10.5194/egusphere-2026-4721
Preprint. Discussion started: 22 September 2026

Wei, Z., Zhang, Z., Vihma, T., Wang, X., and Chen, Y.: An overview of Antarctic polynyas: sea ice production, forcing mechanisms, temporal variability and water mass formation, Adv. Polar Sci., 32, 295–311, https://doi.org/10.13679/j.advps.2021.0026, 2021.

Wernli, H. and Davies, H. C.: A Lagrangian-based analysis of extratropical cyclones. I: The method and some applications, Q. J. R. Meteorol. Soc., 123, 467–489, https://doi.org/10.1002/qj.49712353811, 1997.

Wernli, H. and Schwierz, C.: Surface Cyclones in the ERA-40 Dataset (1958–2001). Part I: Novel Identification Method and Global Climatology, J. Atmos. Sci., 63, 2486–2507, https://doi.org/10.1175/JAS3766.1, 2006.

Yang, K., Wu, J., Li, H., Xu, F., and Zhang, M.: Map of Arctic and Antarctic Polynyas 2013–2022 Using Sea Ice Concentration, Remote Sens., 17, 1213, https://doi.org/10.3390/rs17071213, 2025.

Yin, J. H.: A consistent poleward shift of the storm tracks in simulations of 21st century climate, Geophys. Res. Lett., 32, 2005GL023 684, https://doi.org/10.1029/2005GL023684, 2005.

Zhong, R., Hodges, K., Yang, Q., and Chen, D.: Revisiting the interaction between Antarctic sea ice and Southern Ocean cyclones, J. Geophys. Res., 130, e2024JD042 914, https://doi.org/10.1029/2024JD042914, 2025.